Cancer Research

Small Molecule Inhibition of GDC-0449 Refractory Smoothened Mutants and Downstream Mechanisms of Drug Resistance

Gerrit J. P. Dijkgraaf, Bruno Alicke, Lasse Weinmann, Thomas Januario, Kristina West, Zora Modrusan, Dan Burdick, Richard Goldsmith, Kirk Robarge, Dan Sutherlin, Suzie J. Scales, Stephen E. Gould, Robert L. Yauch, and Frederic J. de Sauvage

Abstract

Inappropriate Hedgehog (Hh) signaling has been directly linked to medulloblastoma (MB), a common malignant brain tumor in children. GDC-0449 is an Hh pathway inhibitor (HPI) currently under clinical investigation as an anticancer agent. Treatment of a MB patient with GDC-0449 initially regressed tumors, but this individual ultimately relapsed with a D473H resistance mutation in Smoothened (SMO), the molecular target of GDC-0449. To explore the role of the mutated aspartic acid residue in SMO function, we substituted D473 with every amino acid and found that all functional mutants were resistant to GDC-0449, with positively charged residues conferring potential oncogenic properties. Alanine scan mutagenesis of SMO further identified E518 as a novel prospective mutation site for GDC-0449 resistance. To overcome this form of acquired resistance, we screened a panel of chemically diverse HPIs and identified several antagonists with potent *in vitro* activity against these GDC-0449–resistant SMO mutants. The bis-amide compound 5 was of particular interest, as it was able to inhibit tumor growth mediated by drug resistant SMO in a murine allograft model of MB. However, focal amplifications of the Hh pathway transcription factor *Gli2* and the Hh target gene cyclin D1 (*Ccnd1*) were observed in two additional resistant models, indicating that resistance may also occur downstream of SMO. Importantly, these HPI resistant MB allografts retained their sensitivity to PI3K inhibition, presenting additional opportunities for the treatment of such tumors. *Cancer Res; 71(2); 435–44. ©2010 AACR.*

Introduction

MB is a primitive neuroectodermal tumor of the cerebellum, which is thought to originate from immature granule neural precursors (GNPs) located in the external granule layer (1). It is the most common brain malignancy among children 0–4 years old and accounts for nearly 18% of pediatric intracranial tumors, with 350 new cases being diagnosed each year in the United States (2). Many patients still succumb to this disease and a large number of survivors suffer from debilitating therapy-related side effects, highlighting the need for alternative therapies.

Hedgehog (Hh) signaling is indispensable for normal embryonic development, yet this pathway is mostly dormant in healthy adults (see ref. 3 for a comprehensive review). Proper signaling is initiated by binding of 1 of 3 Hh ligands (Sonic [SHH], Indian [IHH] or Desert [DHH] Hedgehog) to the inhibitory receptor Patched (PTCH1), which somehow alleviates repression of SMO. Through a series of poorly understood events that at least partly take place in primary cilia, this G-protein coupled receptor (GPCR)–like signal transducer promotes activation of GLI transcription factors that facilitate transcription of Hh target genes. Suppressor of fused (SUFU) is a negative regulator of this pathway and acts by binding directly to GLI transcription factors, affecting both their nuclear trafficking and ability to transcribe DNA. Hh signaling was initially linked to cancer through the discovery that Gorlin Syndrome patients, who have a high incidence of sporadic MB, possess inherited inactivating mutations in *PTCH1* (4). Constitutive Hh signaling has subsequently been shown in 25% of sporadic MBs, with loss of function *PTCH1* or *SUFU* mutations occurring in approximately half of these cases (5, 6).

GDC-0449 is an orally bioavailable SMO antagonist that has produced promising antitumor responses in a Phase I study of patients with advanced basal cell carcinoma (BCC), a type of skin cancer also driven by mutations in Hh pathway components (7). Furthermore, GDC-0449 promptly regressed tumors and reduced symptoms in a 26-year-old man with metastatic MB that was unmanageable by conventional therapies (8). However, the dramatic response of this patient to GDC-0449 treatment was transient, as most of his metastatic tumors

Authors' Affiliation: Genentech Inc., South San Francisco, California

Note: Supplementary data for this article are available at Cancer Research Online (http://cancerres.aacrjournals.org/).

Corresponding Author: Frederic J. de Sauvage, Department of Molecular Biology, Genentech Inc., Mailstop 37, 460 Point San Bruno Blvd, South San Francisco, CA 94080. Phone: 650-225-5841; Fax: 650-225-6497. E-mail: sauvage@gene.com.

doi: 10.1158/0008-5472.CAN-10-2876

recurred, and biopsy of one of these revealed resistance to this HPI due to a mutation in SMO (9).

We report here a novel prospective mutation site in SMO that could also confer resistance to this HPI. We further identify several antagonists with potent activity against these drug resistant SMO mutants, and provide evidence for downstream mechanisms of GDC-0449 resistance. Consequently, overcoming acquired resistance may involve targeting alternative pathways and we show that interfering with PI3K/AKT signaling may be a valid option for HPI-resistant tumors.

Materials and Methods

Alanine scan mutagenesis

SMO mutants were generated from pRK5-*SMO* as described (9). Alanines were mutated to leucine (CTG), whereas all other residues were mutated to alanine (GCA).

[^{3}H]-GDC-0449-binding assays

The 2×10^6 HEK-293 cells were seeded into 10-cm plates and transfected 16 hours later with 3 μg of SMO expression construct using GeneJuice (Novagen). After 40 hours, cells were harvested with PBS containing 1 mmol/L EDTA, fixed with 4% paraformaldehyde for 10 minutes and washed 3 times with PBS. 2×10^5 cells per well were seeded into a 96 well plate and incubated in PBS for 1 hour at 37°C with 5 nmol/L [^{3}H]-GDC-0449 (0.05 μCi) in the presence or absence of 50 μmol/L unlabeled GDC-0449. Cells were transferred to filter plates (Perkin Elmer # 6005174) using a cell harvester (Wallac), washed 6 times and dried. Radioactivity was measured using Microscint-20 scintillation fluid and a Topcount reader (both from Perkin Elmer). Data were either displayed as raw counts, or were normalized to SMO-WT after subtraction of background values (obtained from untransfected cells).

Drug treatment of animals with MB allografts

Tumor-bearing animals were generated via serial subcutaneous propagation of murine *Ptch*$^{+/-}$*; p53*$^{-/-}$ MB tumor lines (10). Subcutaneous tumors 1500–2000 mm^3 were excised from donor mice under aseptic conditions, minced in High Glucose DMEM by repeated slicing and chopping with scalpel blades, and passed through a cell dissociation sieve (Sigma, CD1–1KT). The resulting single-cell suspension was washed twice in High Glucose DMEM and filtered through a 70-μm nylon cell strainer (BD Falcon) before counting in a Vi-CELL cell viability analyzer (Beckman Coulter). Approximately $2.5–10 \times 10^6$ live cells in a 100-μL volume were injected subcutaneously into the right lateral thorax of 7 to 10-week-old female CD-1 nude mice (CRL). Tumor dimensions were measured with Ultra Cal IV calipers (Fred V. Fowler Company Inc.) and tumor volumes were calculated using the formula $v = 0.5 \times a \times b^2$, where a and b are the shortest and longest perpendicular tumor diameters, respectively. When tumors reached 125–350 mm^3, animals were separated into treatment groups with similarly sized tumors and drug administration was initiated. Compounds were formulated in MCT and mice were administered orally 0.2 mL of either vehicle twice daily, compound 5 at 100 mg/kg once daily, or HhAntag at 100 mg/kg twice daily for the HPI study, a single dose of GDC-0449 at 100 mg/kg for the PD study, and either vehicle or GDC-0941 at 150 mg/kg once daily for the PI3K inhibitor study. Mice were euthanized if tumors exceeded 2,000 mm^3 and/or if their body weight dropped >20%. All mice were housed and maintained according to the animal use guidelines of Genentech Inc., conforming to California State legal and ethical practices.

Statistical methods

Log_2(tumor volume) growth traces were fitted to each treatment group with restricted cubic splines for the fixed time effect in each group. Fitting was done via a linear mixed effects model, using the R package "nlme," version 3.1–96 (11) in R version 2.9.2 (R Development Core Team 2008; R Foundation for Statistical Computing; Vienna, Austria).

Hh pathway gene status

Genomic DNA was isolated from tumors with the AllPrep DNA/RNA Mini Kit (Qiagen) and every exon from murine *Smo, Sufu,* and *Gli2* was PCR-amplified using a pair of nested primers containing M13 forward and reverse sequences. Excess primers and free nucleotides were removed with the ExoSAP-IT kit (USB) and PCR products were cycle-sequenced in both directions using M13 sequencing primers, a BigDye Terminator v3.1 Kit and a 3730xl DNA analyzer (both Applied Biosystems). Sequence files were analyzed using Sequencher (GeneCodes) and Mutation Surveyor (SoftGenetics LLC) software.

Gene copy number analyses

Tumor DNA was labeled and hybridized to Mouse Genome 244K CGH Microarrays (Agilent) as per manufacturer recommended protocols, using normal diploid mouse genomic DNA as a reference. Data were normalized with Feature Extraction Software v9.5 (Agilent) and copy number variable regions were called in Nexus 4.0.1 (Biodiscovery) using a rank segmentation algorithm. An arbitrary threshold for copy number gains was set at log2 ratio values of 0.6, with a minimum of 5 probes per segment. Copy number gains were confirmed by qPCR on a MX3000P instrument (Stratagene) using 25 ng of genomic DNA/reaction. Target loci were compared with murine SINE1 elements and quantified on standard curves of normal diploid mouse DNA as described (12) using the following primers:

Gli2 F: 5'-GCAGGACATTCCACACAGTTCTTG-3',
Gli2 R: 5'-ATAGGTGCTGGGATACAGGCTTG-3',
Ccnd1 F: 5'-TACCCTGACACCAATCTCCTCAACG-3',
Ccnd1 R: 5'-GGAATTCCCATCTTCCCAACTCC-3',
Sine1 F: 5'-AGATGGCTGAGTGGGTAAAGG-3' and
Sine1 R: 5'-GTGGAGGTCAGAGGACAAACTT-3'.

Results

D473 is important for SMO inhibition by GDC-0449

We previously reported that mutation of a conserved aspartic acid residue in *SMO* interferes with GDC-0449 binding and its ability to suppress tumor growth, without dramatically altering the signaling activity of this protein (9). To better

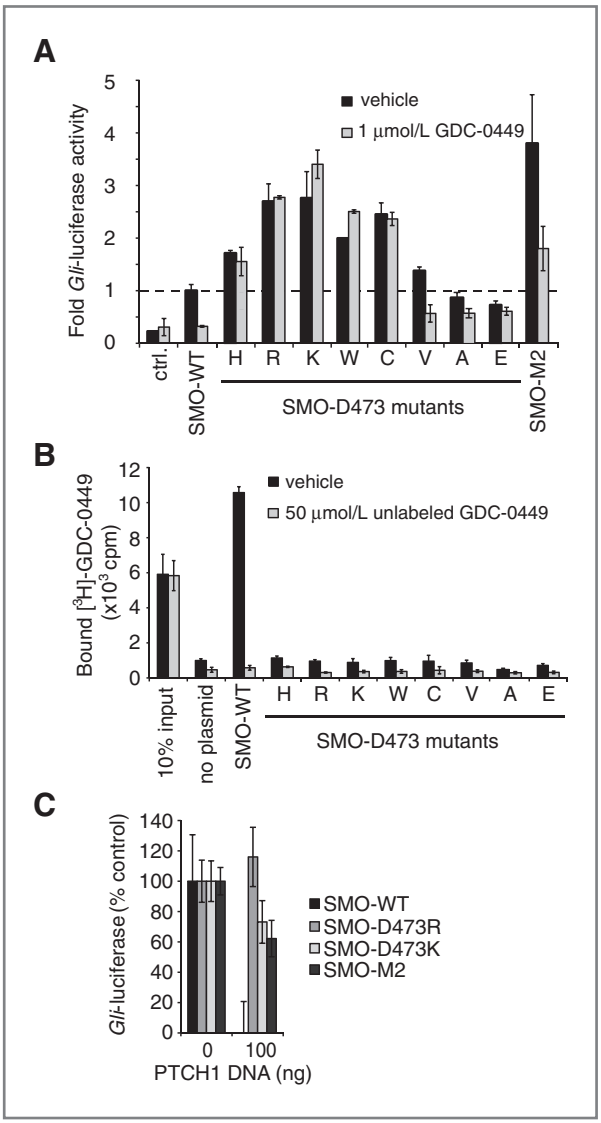

Figure 1. D473 is a key residue in SMO for GDC-0449 binding. A, *Gli*-luciferase activity in CH310T$^1/_2$ cells transfected with wild type or mutant SMO constructs. Values were normalized to those of SMO-WT, Ctrl is GFP and SMO-M2 is SMO-W535L (13). B, binding of [^{3}H]-GDC-0449 to HEK-293 cells transfected with the same SMO plasmids. Drug binding was measured in counts per minute (cpm). *C*, *Gli*-luciferase activity in CH310T$^1/_2$ cells cotransfected with PTCH1 and select SMO constructs. Values were normalized to maximum activity levels of cultures without PTCH1. Data in all experiments are mean ± SD.

characterize the role of D473 in SMO function, we substituted this residue with every amino acid and analyzed the resulting mutants in a *Gli*-luciferase reporter assay in the presence or absence of 1 μmol/L GDC-0449 (Fig. 1A; Supplementary Fig. S1A). Apart from the possibly misfolded SMO-D473P, all mutants induced Hh pathway activity and were less sensitive to GDC-0449 inhibition than SMO-WT. The seemingly responsive D473V mutant was partially drug-resistant in a dose response assay (Supplementary Fig. S1B). Surprisingly, the conservative SMO-D473E mutant was also resistant to GDC-0449, despite maintaining a negative charge at this position. We confirmed cell surface expression for several of these mutants (Supplementary Fig. S1C and D) and tested their ability to bind GDC-0449 (Fig. 1B). Similar to SMO-D473H (9), resistance to this HPI correlated with a lack of SMO-binding, indicating that D473 is critical for SMO inhibition by GDC-0449.

D473 could either be directly involved in GDC-0449 binding or could simply be required to maintain the correct SMO conformation for binding. Several mutants, including those with a positive charge such as D473K and D473R, were more active than SMO-WT and almost as active as the oncogenic SMO-M2 mutant (Fig. 1A; 13), implying that D473 could be a structurally important residue. Consistent with this notion, SMO-D473K and SMO-D473R have autoactivating properties and, like SMO-M2, are resistant to inhibition by PTCH1 (Fig. 1C).

E518 is also important for SMO inhibition by GDC-0449

We used an alanine scan mutagenesis approach to identify additional residues in SMO critical for GDC-0449 binding (Fig. 2A). Assuming that GDC-0449 binds SMO in a manner reminiscent of GPCRs binding to their ligands, we mutated regions known to be important for such interactions (14). These include transmembrane helices (TM) 3, TM5, TM6, and TM7 and adjacent amino acids as well as the entire third extracellular loop of SMO, since it contains D473. We analyzed a total of 102 SMO mutants, using GDC-0449 binding as a primary readout (Supplementary Table S1). Most of the 21 new SMO mutants found to be deficient in GDC-0449 binding were either inactive with respect to signaling or not expressed at the cell surface. However, SMO-E518A showed significant signaling activity despite the presence of 1 μmol/L GDC-0449 and proved to be partially resistant (Fig. 2B). It appears that our binding assay is sensitive to even small changes in drug affinity for SMO, since certain mutants deficient in GDC-0449 binding could still be inhibited at high drug concentrations. We then introduced a more drastic amino acid substitution that reverses the charge at this position and which can be achieved through a single nucleotide change. This SMO-E518K mutant has activity comparable to SMO-WT (Supplementary Table S1), yet is completely resistant to GDC-0449 up to 1 μmol/L (Fig. 2B). Thus, we have identified E518 as a prospective novel mutation site in SMO that could confer resistance to GDC-0449.

A screen of chemically diverse HPIs identified several SMO-D473H and SMO-E518K antagonists

To identify SMO mutant inhibitors as potential therapeutics for GDC-0449–resistant tumors, we screened a panel of 53 antagonists (representative compounds are shown in Fig. 3A) with potent activity against the wild-type protein (Fig. 3B). These inhibitors were either identified in high-throughput screens (both in house and by others) or were generated by hit-to-lead optimization of screening hits using traditional medicinal chemistry methods. The 2 GDC-0449–resistant mutants displayed clearly different requirements for inhibition in our *Gli*-luciferase reporter assay, as SMO-E518K was completely resistant to the natural plant alkaloid cyclopamine

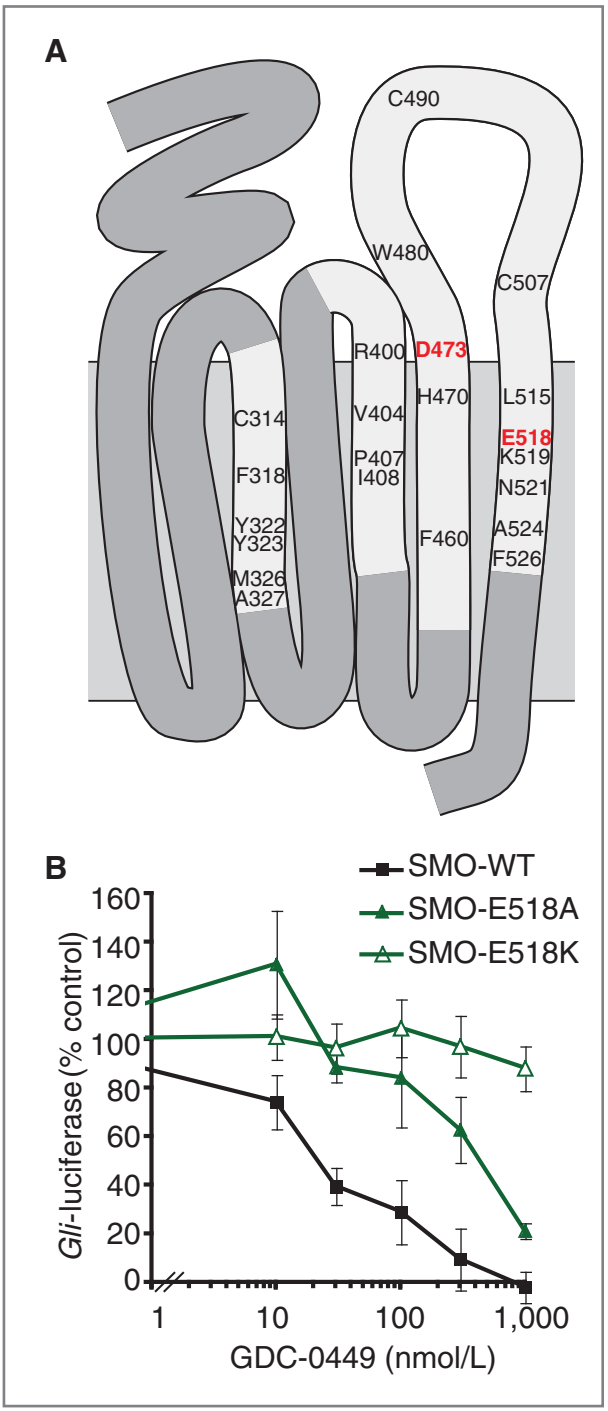

Figure 2. E518 is a novel residue important for SMO inhibition by GDC-0449. A, schematic representation of human SMO. Regions targeted by alanine scan mutagenesis are indicated in light gray. Amino acids important for GDC-0449 binding are shown in black, while residues critical for drug activity are highlighted in red. See Supplementary Table S1 for a comprehensive list of the 102 SMO mutants analyzed. B, *Gli*-luciferase reporter activity of CH310T$^1/_2$ cells transfected with indicated SMO constructs following a dose response of GDC-0449. Values were normalized to maximum activity levels and are mean ± SD.

yet sensitive to the hyrazinoimine SANT-1 (15), while SMO-D473H was partially resistant to both compounds. In addition, various C-ring amide analogs of GDC-0449 had robust potency against SMO-E518K, but were weakly active against SMO-D473H, as exemplified by compound 1 (see Fig. 3A for A-, B-, and C-ring nomenclature). However, the benzimidazole HhAntag (16) was essentially equipotent against all SMO alleles, whereas quinoxalines (represented by compound 2) were found to have low activity against both mutants. Compound 3 showed measurable activity against SMO-D473H despite having an identical C-ring to GDC-0449, and this general class of bis-amides showed improved potencies against both mutants once the optimal substitution pattern was found, exemplified by compound 4.

Although we routinely use HhAntag as a tool compound to block Hh signaling in mice, this inhibitor has a moderate-to-high predicted hepatic clearance based on *in vitro* metabolic stability assays using human liver microsomes and hepatocytes (19 and 12 mL/min/kg, respectively; data not shown), and is therefore suboptimal as a therapeutic agent. To identify a SMO antagonist that might be capable of overcoming acquired GDC-0449 resistance in the clinic, we focused our efforts on the bis-amide class of inhibitors. Three out of 14 drug candidates from this group exhibited good pharmacokinetic properties in mice (data not shown). Of these, we chose to further investigate compound 5, which has a terminal half-life ($t_{1/2}$) of about 22 hours (Fig. 3C) and displayed robust activity against both wild type and SMO-D473H, inhibiting *Gli*-luciferase reporter activity with an IC_{50} of 300 nmol/L and 700 nmol/L, respectively (Fig. 3D). These IC_{50} values are overestimates due to overexpression of SMO in this assay system; the IC_{50} of compound 5 against endogenous human and mouse SMO in the presence of Hh ligand is 8 nmol/L and 27 nmol/L, respectively.

Compound 5 inhibits tumor growth mediated by GDC-0449–resistant SMO

To determine whether compound 5 could inhibit drug resistant SMO *in vivo*, we generated mice with subcutaneous allografts of the murine *Ptch*$^{+/-}$;*p53*$^{-/-}$ MB tumor line SG274. These are resistant to GDC-0449 due to a D477G amino acid substitution in SMO, the same aspartic acid residue that was mutated in human SMO (9). Mice developed 125–350 mm^3 tumors within 2 weeks, after which oral drug treatment was initiated. Although tumor growth in GDC-0449–treated animals did not differ from vehicle, tumors in animals treated with compound 5 not only stopped growing, but even started to shrink during this relatively short time (9; Fig. 4A; Supplementary Figure S2). Tumor growth inhibition was accompanied by a downregulation in *Gli1* mRNA levels (Fig. 4B), indicating that compound 5 can suppress Hh signaling mediated by GDC-0449–resistant SMO *in vivo*. Similar results were obtained with HhAntag at twice the dosing frequency.

GDC-0449 and compound 5 both interfere with SMO translocation to the primary cilium

Recently, several groups reported that diverse antagonists differentially affect the trafficking and localization of SMO to

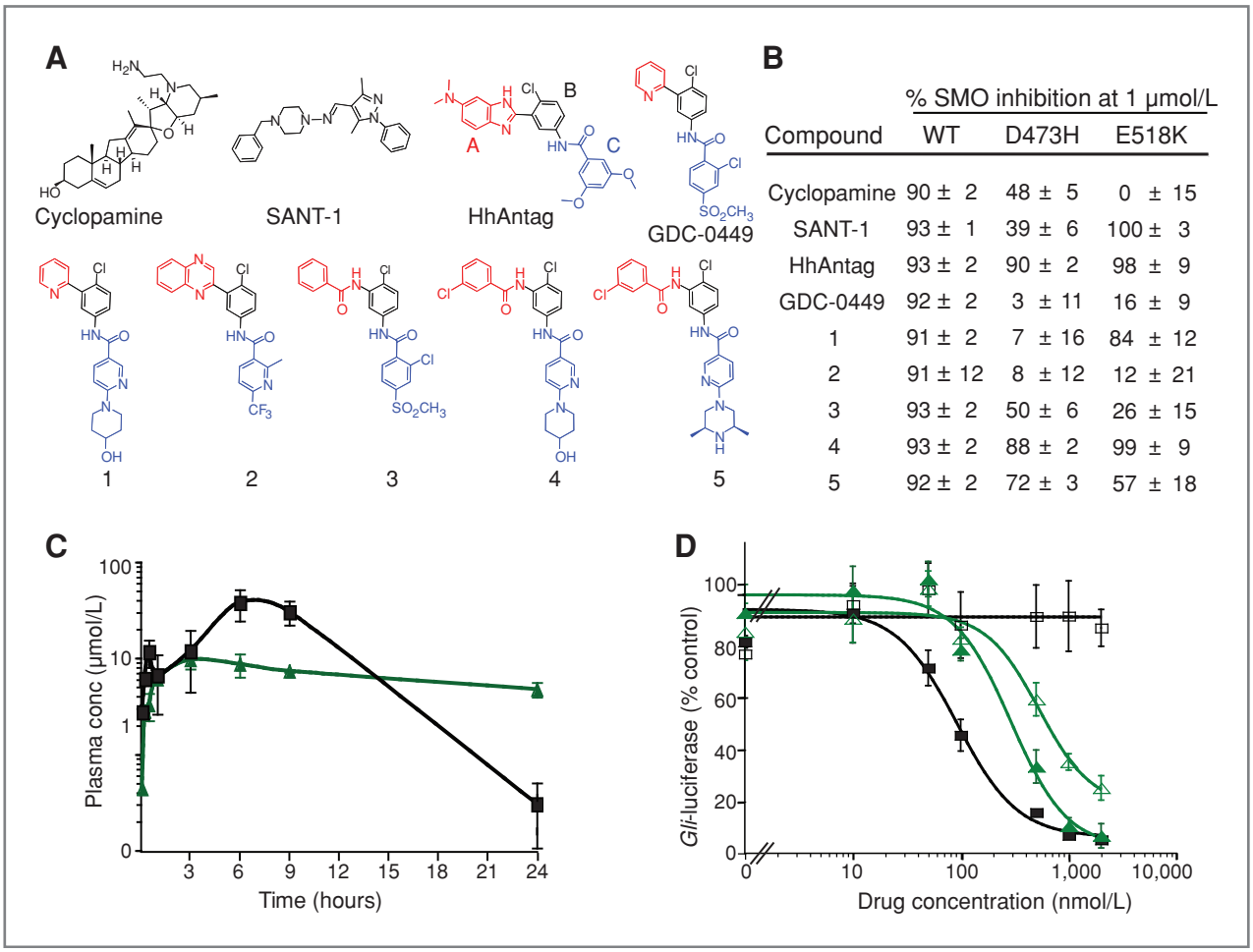

Figure 3. Compound 5 is a potent SMO mutant inhibitor with good pharmacokinetic properties in mice. A, chemical structures of representative SMO antagonists. A red, black, and blue color-coding scheme was used to mark the A-, B-, and C-rings, respectively, of some compounds as indicated for HhAntag. B, % inhibition values of compounds screened at 1 μmol/L. *Gli*-luciferase activity was induced by overexpression of indicated SMO constructs in C3H10T$^1/_2$ cells. C, mean plasma concentration versus time following a single oral 100 mg/kg dose of either compound 4 (black square) or compound 5 (green triangle) in mice ($n = 24$; 3 animals per time point). Note that the structurally similar, but more potent compound 4 has a shorter half life than compound 5 ($t_{1/2}$ of 2$^1/_2$ vs 22 hours). D, relative *Gli*-luciferase reporter activity of C3H10T$^1/_2$ cells transfected with SMO-WT (solid) or SMO-D473H (open) following a dose response of either GDC-0449 (black squares) or compound 5 (green triangles). Data in B to D are mean ± SD.

the primary cilium (17–19). To test the effect of GDC-0449 and the SMO mutant inhibitors on SMO trafficking, we incubated confluent S12 cells with the indicated compounds for 16 hours in the absence or presence of Hh stimulation, and determined whether endogenous SMO colocalized with the primary cilium marker-acetylated tubulin (Fig. 4C and D). Control cells [dimethyl sulfoxide (DMSO), -Hh] displayed very faint SMO staining in only a few cilia. As previously reported (17–19), stimulation with either Shh or the SMO agonist SAG (15) resulted in robust translocation of SMO to the primary cilium, as did cyclopamine treatment. Like SANT-1, GDC-0449 did not promote ciliary enrichment and prevented Hh-induced SMO translocation. Compound 5 and HhAntag had very similar effects to GDC-0449 on SMO localization, suggesting that their ability to inhibit D473H signaling does not involve SMO trafficking. Conversely, KAAD-cyclopamine, a more potent version of cyclopamine (20) that fully inhibits SMO-D473H at 1 μmol/L (9), partially induced ciliary translocation in the absence of ligand (Supplementary Figure S3; Fig. 4D). Addition of Shh did not alter the effect of any compound on SMO localization. In short, we found no obvious correlation between the ability of antagonists to affect SMO localization and their capacity to inhibit GDC-0449–resistant mutants.

GDC-0449 has a differential effect on *Gli1* mRNA expression in 2 additional resistant MB allograft models

We previously reported the establishment of 3 separate drug-resistant MB tumor lines through intermittent dosing with GDC-0449 (9). Only SG274 was found to carry a mutation in *Smo*, indicating that additional mechanisms of resistance to GDC-0449 exist in models SG102 and SG152. Although mutations in the tumor-suppressor *SUFU* predispose individuals to MB (6) and could in theory confer resistance to SMO

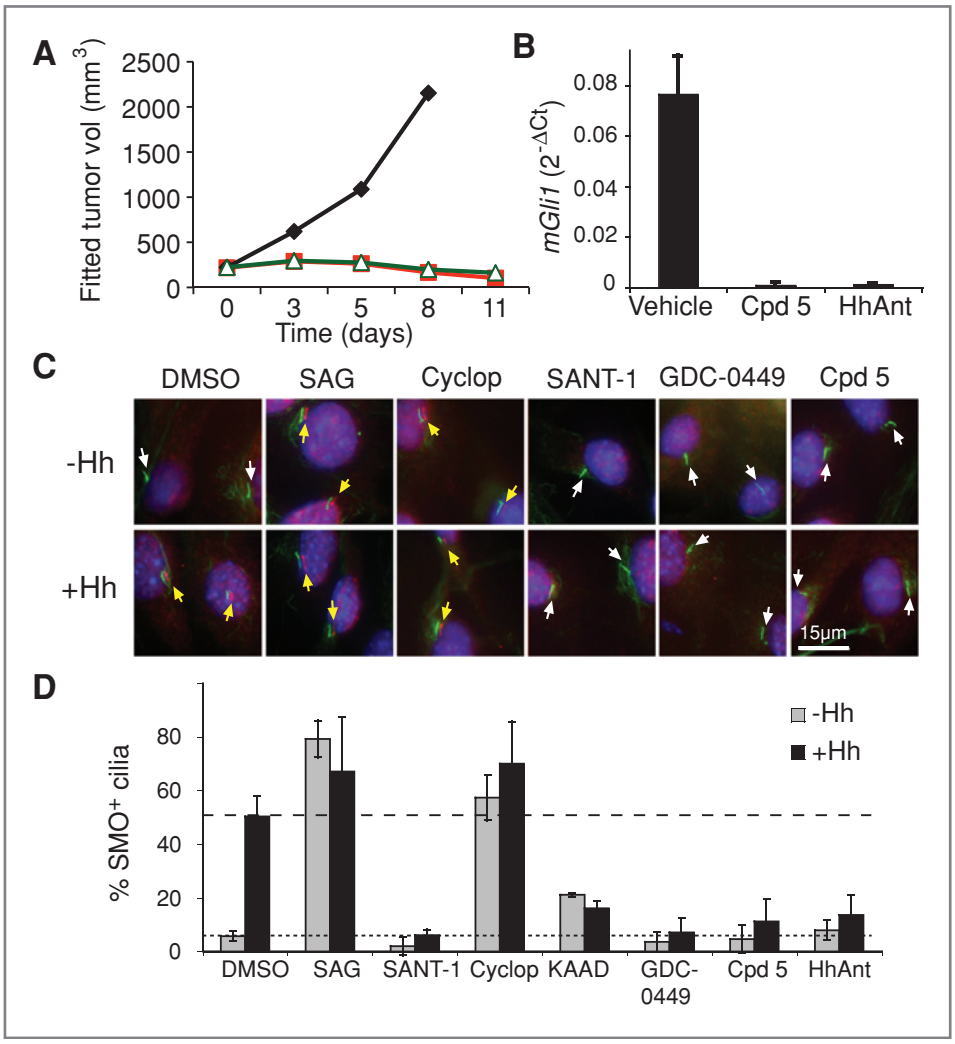

Figure 4. Compound 5 inhibits SMO-D477G–dependent tumor growth and prevents ciliary accumulation of SMO *in vitro*. A, fitted tumor volume of subcutaneous SG274 allografts treated orally with vehicle ($n = 4$, black diamonds), 100 mg/kg compound 5 once daily ($n = 6$, green triangles) or 100 mg/kg HhAntag twice daily ($n = 6$, red squares). Tumor volume traces of individual mice are shown in Supplementary Fig. S2. B, assessment of *mGli1* mRNA levels by qRT-PCR in tumors from panel A collected 6 hours after the last drug treatment. Values represent mean ± SD. C, representative images of S12 cells treated with indicated compounds in the absence (top) or presence (bottom) of Shh for 16 hours. Cilia and centrosomes (acetylated and gamma tubulins respectively, both green) as well as SMO (red) were detected by immunofluorescence, whereas nuclei (blue) were visualized by DAPI staining. A single overlay of all 3 channels is shown with the red (SMO) channel shifted 6 pixels to the right. Arrows point to cilia with robust (yellow) and weak or no (white) SMO staining. Scale bar is 15 μmol/L. D, bar graph depicting the% S12 cells with SMO^+ cilia (yellow arrows in C) under the indicated conditions, calculated from multiple images similar to those shown in panel C.

antagonists, neither model was mutated in this gene. To determine if these tumors had lost their dependence on Hh signaling, we expanded the original resistant tumors and asked whether the Hh pathway was still active in these MB tumor lines (Fig. 5A). *Gli1* levels in vehicle treated, GDC-0449–resistant SG102 or SG152 allografts were comparable to those with control or SMO mutant SG274 allografts, indicating that the Hh pathway is similarly active in all models. Interestingly, GDC-0449 treatment downregulated *Gli1* levels in control and SG102 tumors, but not in SG152 and SG274 tumors. These observations suggest that SG102 and SG152 possess distinct mechanisms of GDC-0449 resistance, independent of *Smo* or *Sufu* mutations and, in the case of SG102, may entail an event downstream of SMO-dependent *Gli* regulation.

Molecular characterization of 2 additional MB allograft models reveals mechanisms of GDC-0449 resistance downstream of SMO

To further investigate the mechanisms of GDC-0449 resistance, we used Comparative Genomic Hybridization (aCGH) to identify potential gene copy number aberrations. Both models contained several regions of copy gains (data not shown), including an amplification of a region on chromosome 7 harboring the Hh target gene cyclin D1 (*Ccnd1*) in model SG102, whereas model SG152 had a high-level focal amplification of a region on chromosome 1 encompassing the Hh pathway transcription factor GLI2 (Supplementary Figure S4). Although cyclin D1 and GLI2 act downstream of SMO and have previously been implicated in the development of MB, we formally cannot rule out involvement of the other genomic alterations in GDC-0449 resistance. The *Ccnd1* and *Gli2* amplifications were independently confirmed by qPCR in SG102 and SG152, when compared with GDC-0449-sensitive control and SMO mutant SG274 tumors (Fig. 5B). These genomic alterations correlated with enhanced mRNA expression and elevated protein levels of both cyclin D1 and GLI2 (Fig. 5B–D). GLI2 contains an aminoterminal repressor domain that when deleted results in a constitutively active protein with 30 times higher transcriptional activity (21). Sequencing of *Gli2* in model SG152 revealed no truncating mutations and both the full-length and repressor forms were detected by immunoblotting, indicating that GLI2 processing

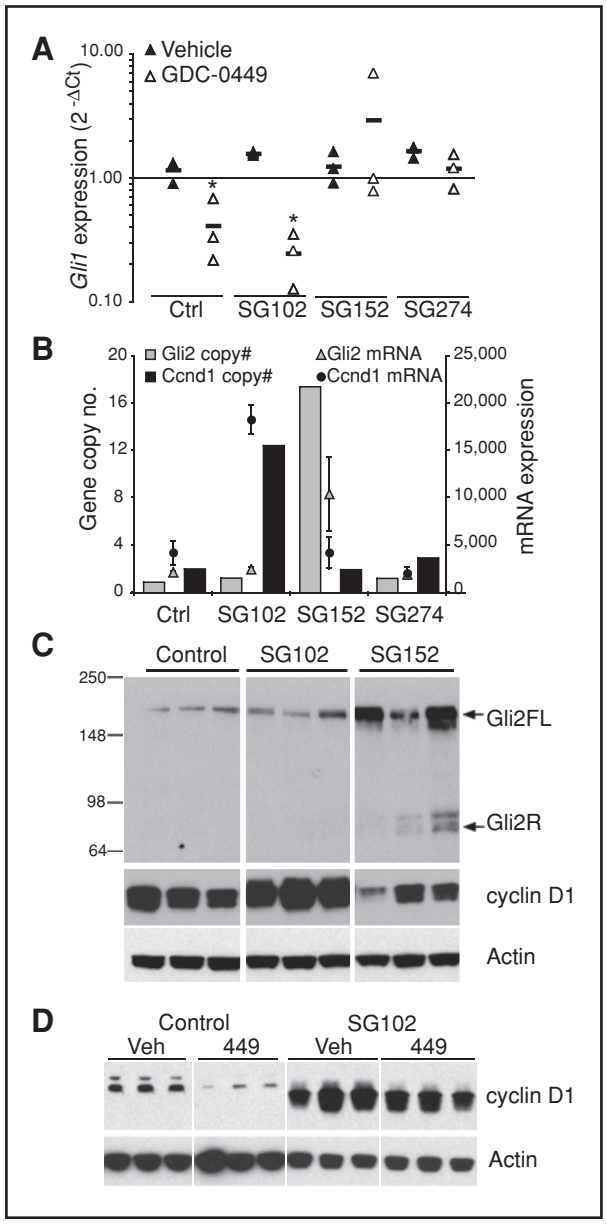

Figure 5. Molecular characterization of additional resistant MB allografts reveals mechanisms of GDC-0449 resistance downstream of SMO. A, quantification of *Gli1* mRNA levels by qRT-PCR in expanded tumors ($n = 3$) collected 6 hours after a single dose with either vehicle (closed triangles) or GDC-0449 (open triangles). * denotes $P < 0.02$. B, graph simultaneously showing the copy number (bars) and mRNA expression (data points) of *Ccnd1* (black) and *Gli2* (gray) in control and GDC-0449–resistant tumors. Gene copy number analysis was done by qPCR of the initial resistant tumor, whereas mRNA expression was determined by micro-array profiling of 3 expanded tumors. Expression levels are shown in arbitrary units and represent mean ± SD. C, immunoblots showing GLI2, cyclin D1 and Actin (loading control) protein levels. Three expanded tumors were analyzed for each line. Gli2FL and Gli2R represent the full length and repressor forms of GLI2. Molecular weight markers are indicated on the left of the GLI2 immunoblot in kilo Daltons (kDa). D, immunoblot showing cyclin D1 levels in expanded control and SG102 tumors ($n = 3$/group) following a 24-hour treatment with either vehicle (Veh) or GDC-0449 (449).

was relatively normal (Fig. 5C). Finally, GDC-0449 down-regulated cyclin D1 levels in control tumors, consistent with *Ccnd1* being an Hh target gene (22), but did not in SG102 tumors (Fig. 5D), despite decreasing *Gli1* mRNA levels (Fig. 5A).

HPI resistant MB allografts are sensitive to PI3K inhibition

Given the identification of resistance mechanisms downstream of SMO, we looked at other signaling pathways implicated in MB to see if targeting any of these might be an alternative therapeutic approach to combating GDC-0449 resistance. Abnormal phosphoinositide3-kinase (PI3K)/AKT signaling promotes tumor growth and survival of many human cancers, including MB (23, 24). We therefore examined the level of activated AKT (phosphorylated at Ser473) and activated S6 (phosphorylated at Ser235/236) in our MB allograft models and were able to detect both phospho-proteins, suggesting that the PI3K/AKT pathway is active in these tumors (Fig. 6A). However, it is unlikely that increased

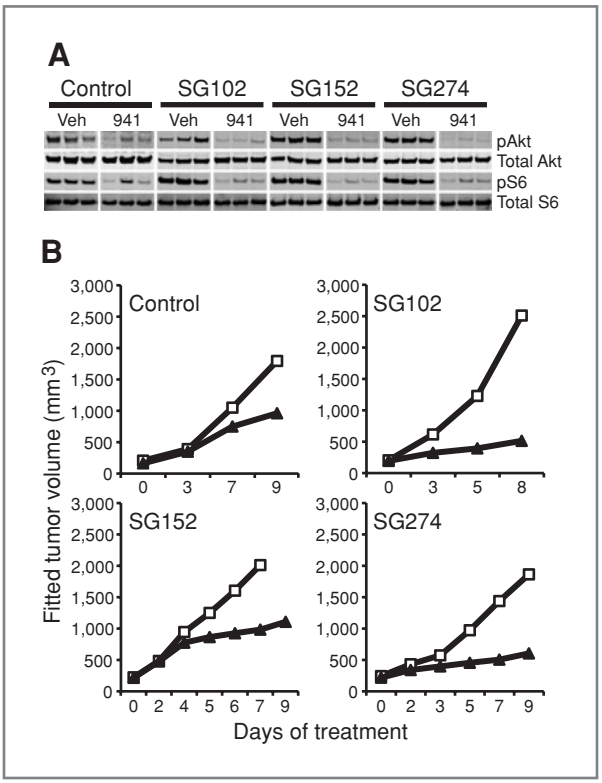

Figure 6. Control and GDC-0449–resistant MB allografts are sensitive to PI3K inhibition. A, immunoblots showing levels of activated AKT and S6 in expanded tumors of the 4 models ($n = 3$/group) following a 6-hour treatment with either vehicle (Veh) or GDC-0941 (941). Total AKT and S6 levels are shown as loading controls. B, mean fitted tumor volumes of control and GDC-0449–resistant MB allografts treated orally with either vehicle (open squares) or 150 mg/kg GDC-0941 once daily (solid triangles). An equal number of animals were analyzed for both treatment arms of each tumor model: Control ($n = 7$), SG102 ($n = 5$), SG152 ($n = 5$) and SG274 ($n = 7$). Tumor volume traces of individual mice are shown in Supplementary Fig. S5.

PI3K/AKT signaling contributes to resistance, since AKT and S6 were also phosphorylated in GDC-0449-sensitive control tumors and an obvious PI3K gene-expression signature (25–27) was lacking in the microarray profiles of the resistant models when compared with sensitive controls (data not shown). Importantly, the PI3K inhibitor GDC-0941 (28) greatly reduced tumor growth in both control and resistant models, indicating that HPI-resistant tumors maintain their dependence on PI3K signaling (Fig. 6B; Supplementary Fig. S5). Tumor growth inhibition in all models was accompanied by PI3K pathway modulation, as GDC-0941 treatment decreased pAKT and pS6 levels (Fig. 6A). However, GDC-0941 treatment only had a limited effect on cyclin D1 levels in SG152 and SG274 tumors (Supplementary Fig. S6), suggesting that the PI3K pathway promotes tumor growth via *Ccnd1*-independent mechanisms in MB, as is the case in GNPs (22). Consequently, pharmacologic inhibition of PI3K/AKT signaling may represent a promising therapeutic approach to treating HPI-resistant MB.

Discussion

SMO is the first GPCR-like protein that has been targeted therapeutically for an oncology indication. As for many other cancer therapies (29), resistance via mutation of the drug target has quickly emerged (9). To better characterize the role of D473 in HPI resistance, we replaced this residue with every amino acid and found that, whereas all functional mutants were GDC-0449-resistant to varying degrees, certain substitutions led to increased signaling, potentially via induction of a conformational change in SMO. Although D473H displayed no significant increase in signaling in our *in vitro* reporter assay, these observations suggest that modification at this site could result in a growth advantage for mutants that may contribute to their emergence prior to drug treatment. Thus mutation of D473 may confer a selective growth advantage *in vivo*.

Using alanine scan mutagenesis of candidate ligand-binding regions, we identified E518 as a novel SMO residue important for inhibition by GDC-0449. Although most mutants deficient in GDC-0449 binding were either inactive or not expressed at the cell surface, alanine substitution of M326, F460, or L515 activated SMO without altering sensitivity to GDC-0449. More drastic amino acid substitutions at these positions may further increase activity and generate GDC-0449–resistant SMO mutants, especially since a previous study showed that cyclopamine resistance positively correlated with the potency of activating SMO mutants (20).

In addition to identifying several potent SMO mutant inhibitors, our screen of chemically diverse HPIs provided some unexpected insights into the binding mode of GDC-0449. Substituting the A-ring of GDC-0449 with one that contains both a hydrogen bond donor and acceptor (as in compound 3) improved potency against SMO-D473H, whereas SMO-E518K was more sensitive to changes in the C-ring (like those introduced by compound 1). It is therefore tempting to speculate that D473 and E518 are part of a GDC-0449 binding site in SMO and interact with the A- and C-ring, respectively. These residues are likely shared with or in close proximity to other binding sites, as several SMO antagonists were less effective against these GDC-0449–resistant mutants. Cocrystallization of SMO with GDC-0449 may be required to elucidate the binding site and precise contribution of these residues.

Rohatgi and colleagues (19) recently proposed a 2-step mechanism for SMO activation, in which full activation of this protein requires ciliary transport coupled to an as yet unidentified second activation step that allows SMO to engage the downstream signaling machinery in cilia. A key concept of their model is that SMO antagonists can be subdivided in 2 classes; "SANT-1-like" inhibitors that influence trafficking of SMO to cilia and "cyclopamine-like" inhibitors that affect the activation step. The authors further proposed that their model might be useful for overcoming drug resistance, anticipating complementary roles for these 2 classes of SMO antagonists in the clinic due to lack of cross-resistance. However, this model does not explain SMO-D473–mediated GDC-0449 resistance. Our data clearly show that inhibitors from the same class can in fact be used to overcome drug-resistance, as the SMO mutant inhibitors compound 5 and HhAntag-affected SMO localization indistinguishably from GDC-0449. Furthermore, antagonists from different classes can display cross-resistance, since neither cyclopamine nor SANT-1 could fully inhibit SMO-D473H. Therefore, an alternative explanation for the distinct effects of HPIs on SMO trafficking may be that antagonists can induce slightly different SMO conformations that favor a particular localization over another, or they could have dissimilar cell permeabilities limiting access to preciliary sites.

Our SMO mutant inhibitors and other HPIs, such as those that antagonize GLI function (30–32), are of limited use if resistance occurs downstream of the molecular target. Indeed, we identified *Ccnd1* and *Gli2* amplification as plausible mechanisms of GDC-0449 resistance downstream of SMO. Both candidate resistance genes have previously been implicated in MB formation. Cyclin D1 promotes proliferation through its ability to bind and stimulate both CDK4 and CDK6, leading to phosphorylation of the retinoblastoma protein and entry into the cell cycle (33). Genetic ablation of *Ccnd1* drastically reduces the incidence of MB in $Ptch^{+/-}$ mice (34), whereas enforced expression of cyclin D1 in $Ink4c^{-/-}$; $p53^{-/-}$ GNPs enabled cells to initiate MBs when injected back into the brains of immunocompromised recipient animals (35). High cyclin D1 levels likely sustain tumor cell proliferation in the presence of GDC-0449, as *Ccnd1* expression is no longer reliant on Hh signaling due to the gene amplification.

Although relatively rare, *GLI2* amplifications have been observed in human MB (36). Tissue-specific expression of a constitutively active form of this transcription factor can lead to MB when ciliogenesis is impaired (37). Furthermore, the oncogenic potential of GLI2 has been firmly established in a mouse model of BCC (38) and viral-mediated expression of the full-length protein allows GNPs to proliferate *in vitro* in the absence of Hh ligand (22).

Similarly, enhanced GLI2 expression by means of gene amplification would render the Hh pathway in tumor cells obviously SMO-independent and therefore GDC-0449 insensitive.

An alternative approach to overcoming acquired resistance is to target other oncogenic pathways such as PI3K/AKT signaling. Human MB samples frequently exhibit activated AKT, and proliferation of human MB cell lines can be attenuated *in vitro* with PI3K inhibitors (24, 39). Furthermore, a recent study reported reduced or absent expression of PTEN, a major inhibitor of the PI3K/AKT pathway, in over half of the human MB samples analyzed (40). Our PI3K inhibitor GDC-0941 was able to greatly reduce the growth of HPI-resistant MB allografts, offering extra opportunities for the treatment of such tumors. Additional studies are required to determine whether combinatorial treatment of MB with GDC-0449 and a PI3K inhibitor can prevent or delay the onset of acquired resistance.

Note: While the article was in review, Buonamici and colleagues (41) also reported Gli2 amplification as a mechanism of resistance to HPI.

Disclosure of Potential Conflicts of Interest

All authors are employees of Genentech, Inc. and F.J. de Sauvage, K. Robarge, and D. Sutherlin hold patents related to Hh signaling.

Acknowledgments

We thank Xiaohui Wen, Celina Rivers, Karen Toy, and Peng Yue for their contributions to this article. We are grateful to Dr. Jonathon Eggenschwiler (Princeton University) for anti-mouse GLI2 antibody and to our colleagues at Curis, Inc. (Cambridge, MA) for HhAntag and other HPIs.

The costs of publication of this article were defrayed in part by the payment of page charges. This article must therefore be hereby marked *advertisement* in accordance with 18 U.S.C. Section 1734 solely to indicate this fact.

Received August 4, 2010; revised October 18, 2010; accepted November 6, 2010; published OnlineFirst December 1, 2010.

References

1. Huse JT, Holland EC. Targeting brain cancer: advances in the molecular pathology of malignant glioma and medulloblastoma. Nat Rev Cancer 2010;10:319–31.
2. Klesse LJ, Bowers DC. Childhood medulloblastoma: current status of biology and treatment. CNS Drugs 2010;24:285–301.
3. Teglund S, Toftgard R. Hedgehog beyond medulloblastoma and basal cell carcinoma. Biochim Biophys Acta 2010;1805:181–208.
4. Hahn H, Wicking C, Zaphiropoulous PG, Gailani MR, Shanley S, Chidambaram A, et al. Mutations of the human homolog of Drosophila patched in the nevoid basal cell carcinoma syndrome. Cell 1996;85:841–51.
5. Zurawel RH, Allen C, Chiappa S, Cato W, Biegel J, Cogen P, et al. Analysis of PTCH/SMO/SHH pathway genes in medulloblastoma. Genes Chromosomes Cancer 2000;27:44–51.
6. Taylor MD, Liu L, Raffel C, Hui CC, Mainprize TG, Zhang X, et al. Mutations in SUFU predispose to medulloblastoma. Nat Genet 2002;31:306–10.
7. Von Hoff DD, LoRusso PM, Rudin CM, Reddy JC, Yauch RL, Tibes R, et al. Inhibition of the hedgehog pathway in advanced basal-cell carcinoma. N Engl J Med 2009;361:1164–72.
8. Rudin CM, Hann CL, Laterra J, Yauch RL, Callahan CA, Fu L, et al. Treatment of medulloblastoma with hedgehog pathway inhibitor GDC-0449. N Engl J Med 2009;361:1173–8.
9. Yauch RL, Dijkgraaf GJ, Alicke B, Januario T, Ahn CP, Holcomb T, et al. Smoothened mutation confers resistance to a Hedgehog pathway inhibitor in medulloblastoma. Science 2009;326:572–4.
10. Wetmore C, Eberhart DE, Curran T. Loss of p53 but not ARF accelerates medulloblastoma in mice heterozygous for patched. Cancer Res 2001;61:513–6.
11. Pinheiro JC, Bates DM. Mixed-effects models in S and S-PLUS. New York: Springer; 2000.
12. Zhao X, Li C, Paez JG, Chin K, Janne PA, Chen TH, et al. An integrated view of copy number and allelic alterations in the cancer genome using single nucleotide polymorphism arrays. Cancer Res 2004;64:3060–71.
13. Xie J, Murone M, Luoh SM, Ryan A, Gu Q, Zhang C, et al. Activating Smoothened mutations in sporadic basal-cell carcinoma. Nature 1998;391:90–2.
14. Rosenbaum DM, Rasmussen SG, Kobilka BK. The structure and function of G-protein-coupled receptors. Nature 2009;459:356–63.
15. Chen JK, Taipale J, Young KE, Maiti T, Beachy PA. Small molecule modulation of Smoothened activity. Proc Natl Acad Sci U S A 2002;99:14071–6.
16. Romer JT, Kimura H, Magdaleno S, Sasai K, Fuller C, Baines H, et al. Suppression of the Shh pathway using a small molecule inhibitor eliminates medulloblastoma in Ptc1(+/-)p53(-/-) mice. Cancer Cell 2004;6:229–40.
17. Wilson CW, Chen MH, Chuang PT. Smoothened adopts multiple active and inactive conformations capable of trafficking to the primary cilium. PLoS One 2009;4:e5182.
18. Wang Y, Zhou Z, Walsh CT, McMahon AP. Selective translocation of intracellular Smoothened to the primary cilium in response to Hedgehog pathway modulation. Proc Natl Acad Sci U S A 2009;106:2623–8.
19. Rohatgi R, Milenkovic L, Corcoran RB, Scott MP. Hedgehog signal transduction by Smoothened: pharmacologic evidence for a 2-step activation process. Proc Natl Acad Sci U S A 2009;106:3196–201.
20. Taipale J, Chen JK, Cooper MK, Wang B, Mann RK, Milenkovic L, et al. Effects of oncogenic mutations in Smoothened and Patched can be reversed by cyclopamine. Nature 2000;406:1005–9.
21. Roessler E, Ermilov AN, Grange DK, Wang A, Grachtchouk M, Dlugosz AA, et al. A previously unidentified amino-terminal domain regulates transcriptional activity of wild-type and disease-associated human GLI2. Hum Mol Genet 2005;14:2181–8.
22. Oliver TG, Grasfeder LL, Carroll AL, Kaiser C, Gillingham CL, Lin SM, et al. Transcriptional profiling of the Sonic hedgehog response: a critical role for N-myc in proliferation of neuronal precursors. Proc Natl Acad Sci U S A 2003;100:7331–6.
23. Vivanco I, Sawyers CL. The phosphatidylinositol 3-Kinase AKT pathway in human cancer. Nat Rev Cancer 2002;2:489–501.
24. Hartmann W, Digon-Sontgerath B, Koch A, Waha A, Endl E, Dani I, et al. Phosphatidylinositol 3'-kinase/AKT signaling is activated in medulloblastoma cell proliferation and is associated with reduced expression of PTEN. Clin Cancer Res 2006;12:3019–27.
25. Saal LH, Johansson P, Holm K, Gruvberger-Saal SK, She QB, Maurer M, et al. Poor prognosis in carcinoma is associated with a gene expression signature of aberrant PTEN tumor suppressor pathway activity. Proc Natl Acad Sci U S A 2007;104:7564–9.
26. Creighton CJ. A gene transcription signature of the Akt/mTOR pathway in clinical breast tumors. Oncogene 2007;26:4648–55.
27. Chang JT, Carvalho C, Mori S, Bild AH, Gatza ML, Wang Q, et al. A genomic strategy to elucidate modules of oncogenic pathway signaling networks. Mol Cell 2009;34:104–14.
28. Folkes AJ, Ahmadi K, Alderton WK, Alix S, Baker SJ, Box G, et al. The identification of 2-(1H-indazol-4-yl)-6-(4-methanesulfonyl-piperazin-1-ylmethyl)-4-morpholin -4-yl-thieno[3,2-d]pyrimidine (GDC-0941) as

a potent, selective, orally bioavailable inhibitor of class I PI3 kinase for the treatment of cancer. J Med Chem 2008;51:5522–32.
29. Tan DS, Gerlinger M, Teh BT, Swanton C. Anti-cancer drug resistance: understanding the mechanisms through the use of integrative genomics and functional RNA interference. Eur J Cancer 2010.
30. Lauth M, Bergstrom A, Shimokawa T, Toftgard R. Inhibition of GLI-mediated transcription and tumor cell growth by small-molecule antagonists. Proc Natl Acad Sci U S A 2007;104:8455–60.
31. Kim J, Lee JJ, Gardner D, Beachy PA. Arsenic antagonizes the Hedgehog pathway by preventing ciliary accumulation and reducing stability of the Gli2 transcriptional effector. Proc Natl Acad Sci U S A 2010;107:13432–7.
32. Hyman JM, Firestone AJ, Heine VM, Zhao Y, Ocasio CA, Han K, et al. Small-molecule inhibitors reveal multiple strategies for Hedgehog pathway blockade. Proc Natl Acad Sci U S A 2009;106:14132–7.
33. Kim JK, Diehl JA. Nuclear cyclin D1: an oncogenic driver in human cancer. J Cell Physiol 2009;220:292–6.
34. Pogoriler J, Millen K, Utset M, Du W. Loss of cyclin D1 impairs cerebellar development and suppresses medulloblastoma formation. Development 2006;133:3929–37.
35. Zindy F, Uziel T, Ayrault O, Calabrese C, Valentine M, Rehg JE, et al. Genetic alterations in mouse medulloblastomas and generation of tumors de novo from primary cerebellar granule neuron precursors. Cancer Res 2007;67:2676–84.
36. Northcott PA, Nakahara Y, Wu X, Feuk L, Ellison DW, Croul S, et al. Multiple recurrent genetic events converge on control of histone lysine methylation in medulloblastoma. Nat Genet 2009;41:465–72.
37. Han YG, Kim HJ, Dlugosz AA, Ellison DW, Gilbertson RJ, Alvarez-Buylla A. Dual and opposing roles of primary cilia in medulloblastoma development. Nat Med 2009;15:1062–5.
38. Grachtchouk M, Mo R, Yu S, Zhang X, Sasaki H, Hui CC, et al. Basal cell carcinomas in mice overexpressing Gli2 in skin. Nat Genet 2000;24:216–17.
39. Baryawno N, Sveinbjornsson B, Eksborg S, Chen CS, Kogner P, Johnsen JI. Small-molecule inhibitors of phosphatidylinositol 3-kinase/Akt signaling inhibit Wnt/beta-catenin pathway cross-talk and suppress medulloblastoma growth. Cancer Res 2010;70:266–76.
40. Castellino RC, Barwick BG, Schniederjan M, Buss MC, Becher O, Hambardzumyan D, et al. Heterozygosity for Pten promotes tumorigenesis in a mouse model of medulloblastoma. PLoS One 2010;5:e10849.
41. Buonamici S, Williams J, Morrissey M, Wang A, Guo R, Vattay A, et al. Interfering with resistance to smoothened antagonists by inhibition of the PI3K pathway in medulloblastoma. Sci Transl Med 2010;2:51ra70.